

Exploring phases of the Su-Schrieffer-Heeger model with tSNE

R. M. Woloshyn

TRIUMF, 4004 Wesbrook Mall, Vancouver, British Columbia, Canada V6T 2A3

T-distributed stochastic neighborhood embedding (tSNE) is used as a tool to reveal the phase diagram of the Su-Schrieffer-Heeger model and some of its extended and non-Hermitian variants. Bloch vectors calculated at different points in the parameter space are mapped to a two-dimensional reduced space. The clusters in the reduced space are used to visualize different phase regions included in the input. The tSNE mapping is shown to be effective even in the challenging case of the non-Hermitian extended model where five different phases are present. An example of using wavefunction input, instead of Bloch vectors, is presented also.

I. INTRODUCTION

Machine learning is being increasingly utilized in physics [1, 2]. Examples of applications include event classification [3–5] and anomaly detection [6, 7] in the analysis of particle physics experiments, aiding observations in astronomy [8], and the study of phases in condensed matter systems [9–12]. The focus here on the last topic, phases of matter.

Many different machine learning methods have been applied to the exploration of phases and phase transitions. These include neural networks [13–16], principal component analysis [17, 18], support vector machines [19] and diffusion maps [20–22]. In an interesting recent work, Yang *et al.* [23] suggested the use of t-distributed stochastic neighborhood embedding (tSNE) as an unsupervised learning method to obtain a visualization of phase diagrams and used this method to study a number of one-dimensional quantum spin systems.

The idea of using unsupervised learning methods to reveal phases is particularly appealing. Specifically, topological phases [24] which can not be characterized by local order parameters can be studied without *a priori* input of domain knowledge. Ref. [21, 22, 25–30] are examples of recent work on identifying topological phases and phase transitions using either neural networks or diffusion maps. The Ref. [22, 25–29] focus on the Su-Schrieffer-Heeger (SSH) model [31, 32] which is also the subject of this work.

The SSH model was introduced as a model for polyacetylene and is a simple extensively studied example of a model for a topological insulator [33, 34]. The basic model consists of electrons (taken to be spinless) hopping on a one-dimensional lattice. The nearest-neighbor hopping amplitudes are taken to be staggered (see, for example, Fig. 1.1 in [33]) so the lattice can be divided into two-site units cells. Some details of the model are given in Sec. III.

The SSH model can be extended by introducing longer range interactions. The extended SSH model considered here allows for the addition of next-next-nearest neighbor hopping terms [28, 35]. A different type of modification of the model which has received considerable recent attention is to allow nonreciprocal intra-cell hopping [36, 37]. This leads to a non-Hermitian Hamiltonian and the appearance of topological phases with fractional winding number [37].

In this paper the tSNE algorithm, which has been used to study one-dimensional spin systems [23], is applied to the SSH model and the variants mentioned above. The algorithm is based on dimensionality reduction. The model, sampled at a variety of points in its parameter space, is described by points distributed in a high-dimensional space and tSNE maps this space to a lower-dimensional space where, ideally, there is a clustering of data which can be used to identify regions of parameter space which share common features. In this work a model which allows calculations to be made for different parameters but the same strategy can be applied to data from experiments where measurements are made under different experimental conditions.

The implementation of tSNE analysis requires choices to be made, for example, for a distance function for points in the high-dimensional input space and for the algorithm to identify clusters in the tSNE output. These issues are discussed in Sec. IV and in the Appendices. With appropriate choices it is found that the unsupervised tSNE analysis can give a correct visualization of the phase diagram even the most challenging case of the non-Hermitian extended SSH model where five phases are present.

The tSNE algorithm is introduced in Sec. II and Sec. III gives a brief outline of the SSH model and some of its extensions. Results are presented in Sec. IV with a summary in Sec. V.

II. T-DISTRIBUTED STOCHASTIC NEIGHBORHOOD EMBEDDING

T-distributed stochastic neighborhood embedding [38] (tSNE) is based on the notion of dimensionality reduction. The system to be analyzed is described by a set of points $\{\mathbf{x}\}$ in a space with large dimension which may obscure the presence features with a much smaller dimensionality. The idea of tSNE is to construct a mapping of $\{\mathbf{x}\}$ to points

$\{\mathbf{y}\}$ in a space of low dimension (typically 2 or 3) in such a way that points in the high-dimensional space that share some common feature will lie close together in the low-dimensional space.

A key element of tSNE, common to other some machine learning algorithms, for example, diffusion maps, is the distance $D_{ij}(\mathbf{x}_i, \mathbf{x}_j)$ between points in the high-dimensional space. The distance D is commonly taken to be the Euclidean distance between the points but other metrics can be used and, depending on the application, may be more effective. The first step of the algorithm is to assign a conditional probability that point i should have point j as a neighbor

$$P_{j|i} = \frac{e^{-D_{ij}^2/2\sigma_i^2}}{\sum_{k \neq i} e^{-D_{ik}^2/2\sigma_i^2}}, \quad (1)$$

for all $i \neq j$. The σ_i 's are hyperparameters of the algorithm. Then a probability P_{ij} is defined by

$$P_{ij} = \frac{P_{i|j} + P_{j|i}}{2N}, \quad (2)$$

where N is the number of points in the set $\{\mathbf{x}\}$.

A probability distribution Q_{ij} for points $\{\mathbf{y}\}$ in the low-dimensional space is also defined. It is taken to be a Student t-distribution

$$Q_{ij} = \frac{\left[1 + \|\mathbf{y}_i - \mathbf{y}_j\|^2\right]^{-1}}{\sum_{k \neq i} \left[1 + \|\mathbf{y}_i - \mathbf{y}_k\|^2\right]}, \quad (3)$$

using Euclidean distance. The algorithm then tries to make the probability distribution Q similar to P by find points $\{\mathbf{y}\}$ which minimize the Kullback-Leibler divergence defined by

$$\sum_{ij} P_{ij} \log \frac{P_{ij}}{Q_{ij}}. \quad (4)$$

The tSNE algorithm is included in the machine learning toolkit scikit-learn [39, 40] and that is the implementation that will be used in this work. In the implementation of tSNE the hyperparameters are fixed implicitly by requiring that the so-called perplexity \mathcal{P} , defined by

$$\log_2 \mathcal{P} = - \sum_j P_{j|i} \log_2 P_{j|i}, \quad (5)$$

takes a specified value.

III. THE SU-SCHRIEFFER-HEEGER MODEL

The SSH model was introduced as a model for polyacetylene [31, 32]. It consists of electrons hopping on one-dimensional lattice with a two-site unit cell. The intra-cell and inter-cell couplings are taken to be different. The Hamiltonian for the basic model with L unit cells is

$$H = \sum_{j=1}^L \left[t_1 a_j^\dagger b_j + t_2 a_{j+1}^\dagger b_j \right] + h.c. \quad (6)$$

where a_i^\dagger and b_i denote creation and annihilation operators on the two different sites of the i 'th unit cell. With periodic boundary conditions the Hamiltonian can be written in momentum space as

$$H(k) = d_x(k)\sigma_x + d_y(k)\sigma_y, \quad (7)$$

where the σ 's are Pauli matrices and the Bloch vectors are

$$\begin{aligned} d_x(k) &= t_1 + t_2 \cos(k), \\ d_y(k) &= t_2 \sin(k). \end{aligned} \quad (8)$$

The momenta k take values in $[0, 2\pi]$. The SSH model has a nontrivial topological property. If $t_2 > t_1$ the vector $\mathbf{d} = (d_x, d_y)$ will rotate about the origin of the $d_x - d_y$ plane as k varies from 0 to 2π (see, for example, Fig. 8 in Ref [34]). Note that the trajectory of the Bloch vectors passing through the point $\mathbf{d} = 0$ is the condition that the model is gapless Ref [37]. This can occur when $t_1 = \pm t_2$ which is the boundary in parameter space between different phases. When $t_2 > t_1$ the winding number $w = 1$ where for our discretized lattice

$$w = \frac{1}{2\pi} \sum_j^L \Delta\phi(j), \quad (9)$$

where $\Delta\phi(j) = |\phi(j) - \phi(j-1)| \bmod 2\pi$ with ϕ_j equal to the phase of $d_x(k) + id_y(k)$ for $k = 2\pi j/L$. When $t_2 < t_1$, the winding number vanishes.

The SSH model can be extended to include next-to-next-nearest neighbor inter-cell hopping and the coupling between nearest neighbor cells and next-to-next-nearest neighbor cells can be taken to be different. In this case the Bloch vectors take the form

$$\begin{aligned} d_x(k) &= t_1 + t_2 \cos(k) + t_3 \cos(2k), \\ d_y(k) &= t_2 \sin(k) + t_3 \sin(2k). \end{aligned} \quad (10)$$

In this case the vector \mathbf{d} will trace out a double loop in the $d_x - d_y$ plane and the winding number can take values 0, 1 or 2 (See, for example, [28, 35]).

Another extension of the SSH model is to allow for a non-reciprocal inter-cell hopping strength. This leads to a non-Hermitian Hamiltonian. In the non-Hermitian extension considered here the Bloch vectors take the form [29, 37]

$$\begin{aligned} d_x(k) &= t_1 + t_2 \cos(k), \\ d_y(k) &= t_2 \sin(k) - i\delta, \end{aligned} \quad (11)$$

where δ is a real parameter characterizing the difference between left and right intra-cell hopping. The condition for the energy gap to vanish becomes $t_1 = \pm t_2 \pm \delta$. In addition to phases with winding number 0 and 1, there are regions of parameter space where $w = 1/2$.

The extended SSH model (10) can also be modified to include non-Hermiticity. The Bloch vectors become [37]

$$\begin{aligned} d_x(k) &= t_1 + t_2 \cos(k) + t_3 \cos(2k), \\ d_y(k) &= t_2 \sin(k) + t_3 \sin(2k) - i\delta. \end{aligned} \quad (12)$$

The phase diagram becomes quite complicated with regions of winding number 1/2 and 3/2 appearing along with winding numbers 0, 1 and 2 that are present when $\delta = 0$.

IV. RESULTS

A. Bloch vector input

In this section results of applying the tSNE reduction to the SSH models of Section are described. The Bloch vectors calculated at different points lying in a two-dimensional plane of parameter space and spanning different phases are used as input into the algorithm. The reduced space is taken to be two-dimensional. As mentioned in Sec. II the distance function in the space of input vectors need not be the Euclidean distance. Scikit-learn provides a variety of metrics. In this work the \mathbb{L}_p norms with $p = 1, 2, \infty$ were considered. In scikit-learn these are called Cityblock, Euclidean and Chebyshev respectively. Recall that the \mathbb{L}_p norm of a vector \mathbf{v} is

$$\mathbb{L}_p = \left(\sum_i |v_i|^p \right)^{\frac{1}{p}}. \quad (13)$$

If the number of clusters to which the data are mapped is very small the choice of metric may not be critical. However, if, for example, the input data span a large number phases some metrics may be more effective than others. The example in Appendix A Fig. 6 of the non-Hermitian extended SSH model shows that using the Chebyshev distance leads to well separated clusters while other choices do not. All results presented in this Section based on Bloch vector input were calculated using the Chebyshev distance. Note the use of this metric was earlier advocated by Che *et al.* [25] in their study topological phases using diffusion maps.

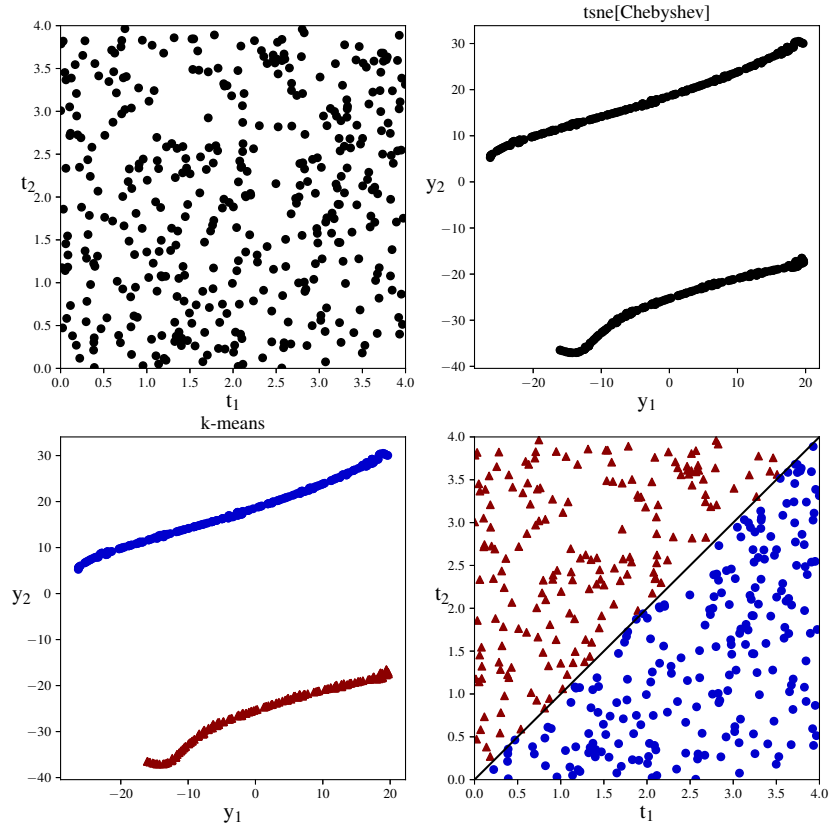


Figure 1. Phases of the SSH model exposed by tSNE. Top-left: Points in the $t_1 - t_2$ parameter space at which input Bloch vectors are calculated. Top-right: Output of tSNE. Bottom-left: Clusters identified by k-means. Bottom-right: Points in parameter space with color and symbol showing the cluster to which they correspond. The black line shows the known phase boundary.

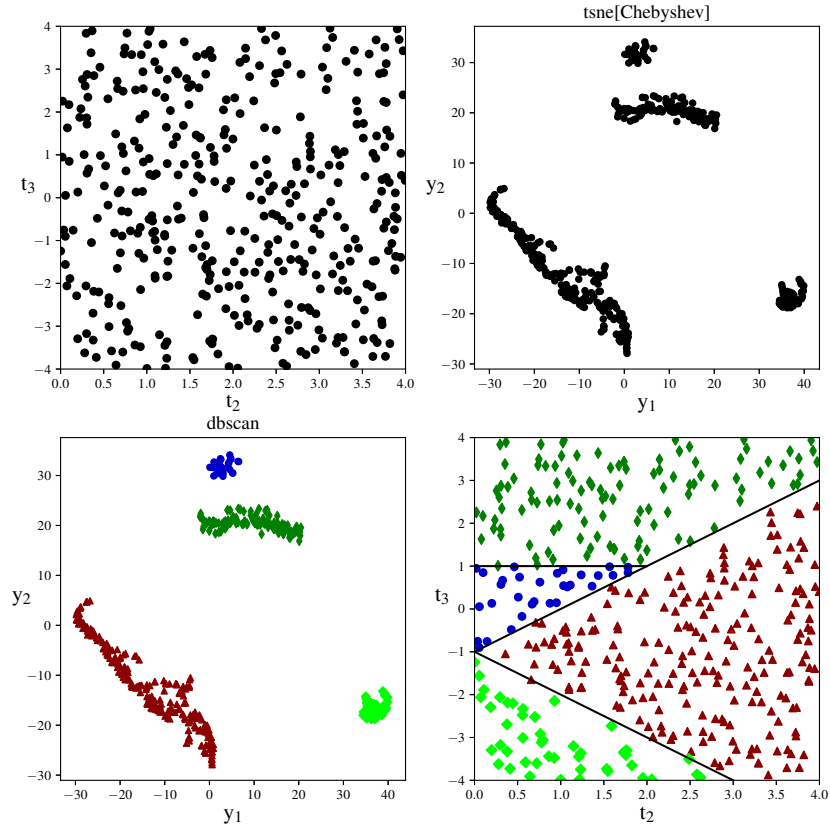


Figure 2. Phases of the extended SSH model exposed by tSNE. Top-left: Points in the $t_2 - t_3$ parameter space with $t_1 = 1$ at which input Bloch vectors are calculated. Top-right: Output of tSNE. Bottom-left: Clusters identified by dbSCAN. Bottom-right: Points in parameter space with color and symbol showing the cluster to which they correspond. The black lines show the known phase boundaries.

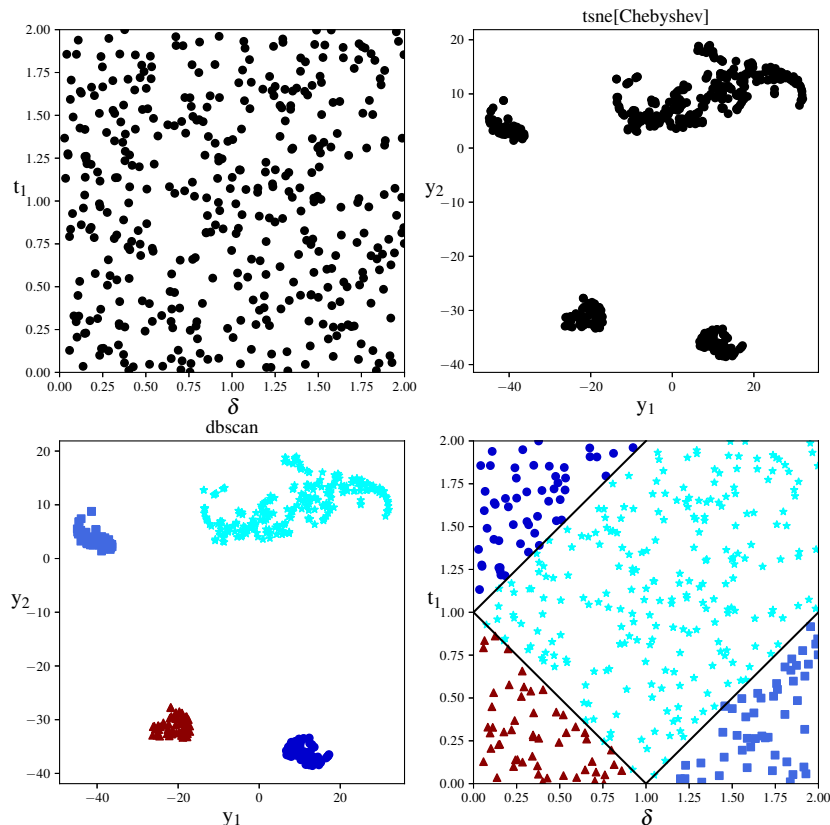


Figure 3. Phases of the non-Hermitian SSH model exposed by tSNE. Top-left: Points in the $\delta - t_1$ parameter space with $t_1 = 1$ at which input Bloch vectors are calculated. Top-right: Output of tSNE. Bottom-left: Clusters identified by dbscan. Bottom-right: Points in parameter space with color and symbol showing the cluster to which they correspond. The black lines show the known phase boundaries.

First consider the basic SSH model Eq. 8. The model has two parameters. A sample of 400 Bloch vectors corresponding to a lattice of 80 cells was constructed using parameters chosen randomly in the range $0 \leq t_1, t_2 \leq 4$. The selected points are shown in the top-left panel of Fig. 1. The result of tSNE mapping of the Bloch vectors to a two-dimensional space using the Chebyshev distance is shown in the top-right panel of the figure. The default value of the perplexity, $\mathcal{P} = 30$, was used. Two clusters can be identified by inspection or by using a clustering algorithm such as k-means [41]. The clusters, coded by color and symbol, are displayed in the bottom-left panel. The points in parameter space are replotted in the bottom-right panel now coded with color and symbol indicating the cluster to which they were grouped by tSNE. The diagonal line is the phase boundary between the topological phase $t_2 > t_1$ with winding number equal to 1 and the band insulator phase $t_2 < t_1$ with winding number 0. One sees that tSNE makes a clear separation of the phases in an unsupervised way giving a visualization of the phase diagram.

The extended SSH model, Eq. 10, has three parameters. We consider the model at $t_1 = 1$ and allow the other parameters to vary in the range $0 \leq t_2 \leq 4$ and $-4 \leq t_3 \leq 4$. The randomly selected points are shown in the top-left panel of Fig. 2 and the tSNE output is in the top-right panel. This model has a more complicated phase diagram than the basic SSH model (see Fig. 5 in [28]) and the choice of clustering algorithm becomes an issue. The results of using k-means clustering are compared to dbscan [41, 42] in Appendix B Fig. 8. The dbscan clusters, coded with different colors and symbols, are shown in the bottom-left of panel Fig. 2. The corresponding points in the $t_2 - t_3$ plane along with the known phase boundaries [28] are plotted in the bottom-right panel. The tSNE analysis gives a clean separation of the phase diagram into four regions in agreement with known results. Note that this would not be the case if k-means were used for cluster identification.

The phase diagram of the non-Hermitian SSH model, Eq. 11, is shown in Fig. 3 of Ref. [37] for $t_2 = 1$. For this work we consider a quadrant of the parameter space with $0 \leq \delta, t_1 \leq 2$. The input Bloch vectors were calculated at the 400 points plotted in the top-left panel of Fig. 3 and top-right panel shows the tSNE output. Cluster identification using dbscan is shown in the bottom-left panel. The four distinct regions in the parameter space are correctly identified (bottom-right panel) as indicated by the black lines showing the phase boundaries.

The non-Hermitian extended SSH model, Eq. 11, presents more of a challenge. There are five phases with different

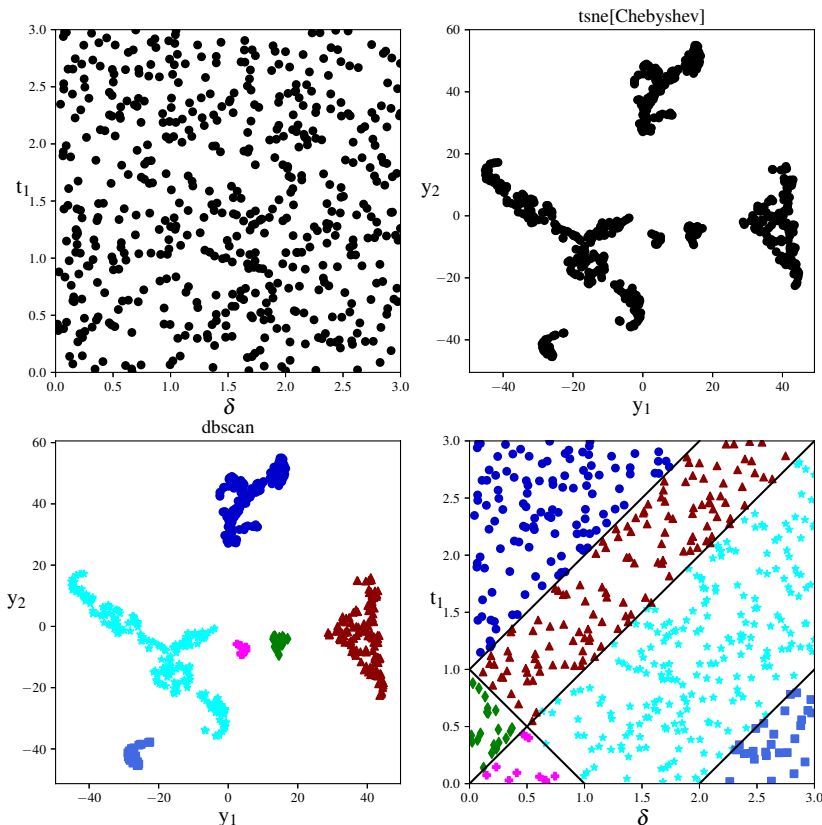


Figure 4. Phases of the non-Hermitian extended SSH model exposed by tSNE. Top-left: Points in the $\delta - t_1$ parameter space with $t_2, t_3 = 1$ at which input Bloch vectors are calculated. Top-right: Output of tSNE. Bottom-left: Clusters identified by dbSCAN. Bottom-right: Points in parameter space with color and symbol showing the cluster to which they correspond. The black lines show the known phase boundaries.

winding numbers. The phase diagram in the $\delta - t_1$ plane for $t_2, t_3 = 1$ is given in Fig. 5 of Ref. [37]. Here 529 points in the range $0 \leq \delta, t_1 \leq 3$ are used for the input Bloch vectors. These are shown in the top-left panel of Fig. 4 and the resulting tSNE mapping is in the top-right panel. A perplexity of 20 was used in this case as it was found to give a better separation of the clusters than the default value of 30. The dbSCAN identification of clusters, depicted in different colors and symbols, is in the lower-left panel. The bottom-right panels shows the points in the $\delta - t_1$ plane associated with different clusters. Phase boundaries are shown by the black lines. It seems quite remarkable that the combination of tSNE dimensionality reduction and dbSCAN clustering can distinguish all six regions even though some are small and represented by only a few points in the input sample.

B. Wavefunction input

An alternative to using the Bloch vectors to explore the phases is to use the eigenvectors of the real-space Hamiltonian. For a lattice of L cells the Hamiltonian can be expressed as an $2L \times 2L$ sparse matrix with nonzero entries along the super- and sub-diagonal [33]. Let $|\psi_i\rangle$ and $|\psi_j\rangle$ denote the lowest positive energy eigenvectors for two different choices of the model parameters. An \mathbb{L}_p norm of the difference between these vectors can be used as a distance in an tSNE analysis but this may not be the best choice. Yang *et al.* [23] suggest that for visualizing quantum phases with tSNE a better measure of distance between quantum states would be

$$-\log |\langle \psi_i | \psi_j \rangle| \quad (14)$$

which they call the negative logarithmic fidelity (NLF). As an example, Fig. 7 in Appendix A shows the tSNE reduction using a sample of 400 SSH model wavefunctions calculated on a lattice of 16 cells for different randomly chosen t_1 and t_2 values. Since the model has two phases two clusters of points in the $y_1 - y_2$ plane are expected. With an \mathbb{L}_p norm one sees two clusters of outliers in addition to the main clusters which makes the association of clusters with phases problematic. With NLF there is a clear separation into reasonably compact clusters. The complete

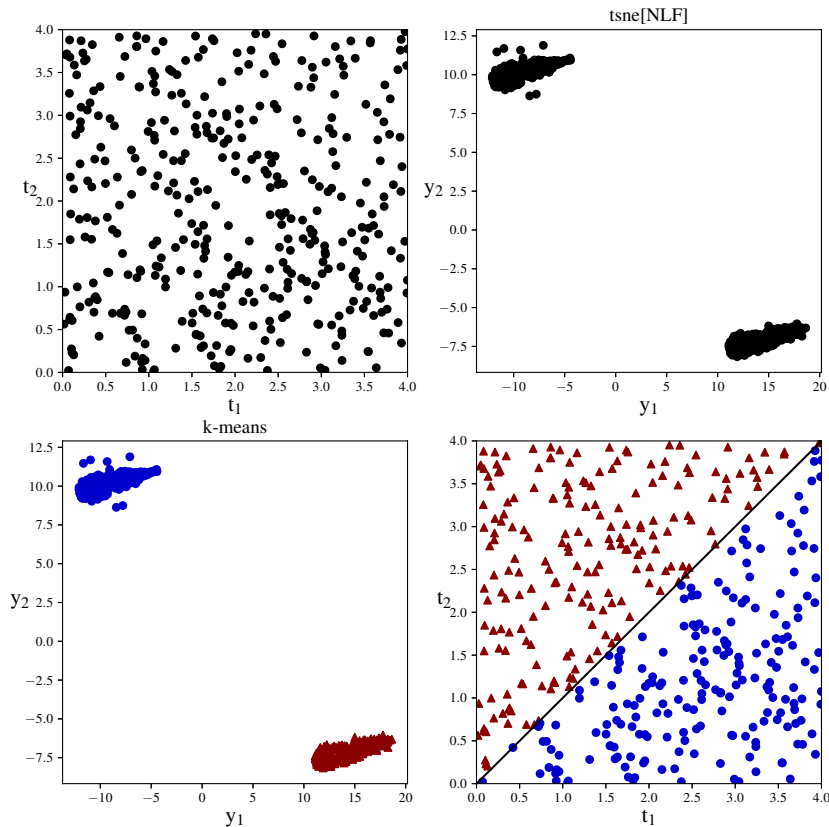


Figure 5. Phases of the SSH model exposed by tSNE with wavefunction input. Top-left: Points in the $t_1 - t_2$ parameter space at which input wavefunctions are calculated. Top-right: Output of tSNE. Bottom-left: Clusters identified by k-means. Bottom-right: Points in parameter space with color and symbol showing the cluster to which they correspond. The black line shows the known phase boundary.

analysis with wavefunction input using NLF is shown in Fig. 5. The two phases are clearly distinguished just as in Fig. 1 where Bloch vectors were used.

V. SUMMARY AND DISCUSSION

Machine learning offers many ways of exploring phase transitions in condensed matter systems. Particularly interesting are unsupervised methods which require no *a priori* knowledge such as a choice of an order parameter. Such methods are especially suited to the study of topological phase transitions where there is no local order parameter.

In this work it is shown that t-distributed Stochastic Neighborhood Embedding it is can be used to learn the phase boundaries of the Su-Schrieffer-Heeger model and some of its extensions. Input into the analysis consists of Bloch vectors constructed at different points of the model parameter space. The tSNE algorithm was used to map the Bloch vectors to clusters in a reduced space (two-dimensional in this work) corresponding to different regions of the phase diagram. This allows a visualization of the phase diagram as shown in Figs. 1 to 4. Wavefunction input can also be used in the analysis as shown in Fig. 5.

tSNE does not work automatically. The choice of distance function used to construct the probability distribution of the input can affect the results. For Bloch vector input, the Chebyshev distance was preferred since it worked well even in the difficult case of the non-Hermitian extended SSH model. With wavefunction input, negative logarithmic fidelity [23] was found to be useful whereas \mathbb{L}_p norms did not produce usable even in the simple case with only two phases. As well, the perplexity may require some adjustment to get a good separation of the clusters in the reduced space. Since tSNE is stochastic, the output varies from run to run so making adjustments to the algorithm requires some care.

Although tSNE can be used to identify regions in different phases, it can not find the properties, such as the winding number, associated to different regions. This is true also for other machine learning methods, for example, principal component analysis or diffusion maps, used to expose phase boundaries. Nonetheless, since these learning algorithms

are unsupervised, they can provide useful information about phase transitions without input of domain knowledge.

ACKNOWLEDGMENTS

TRIUMF receives federal funding via a contribution agreement with the National Research Council of Canada.

Appendix A: Choice of metric

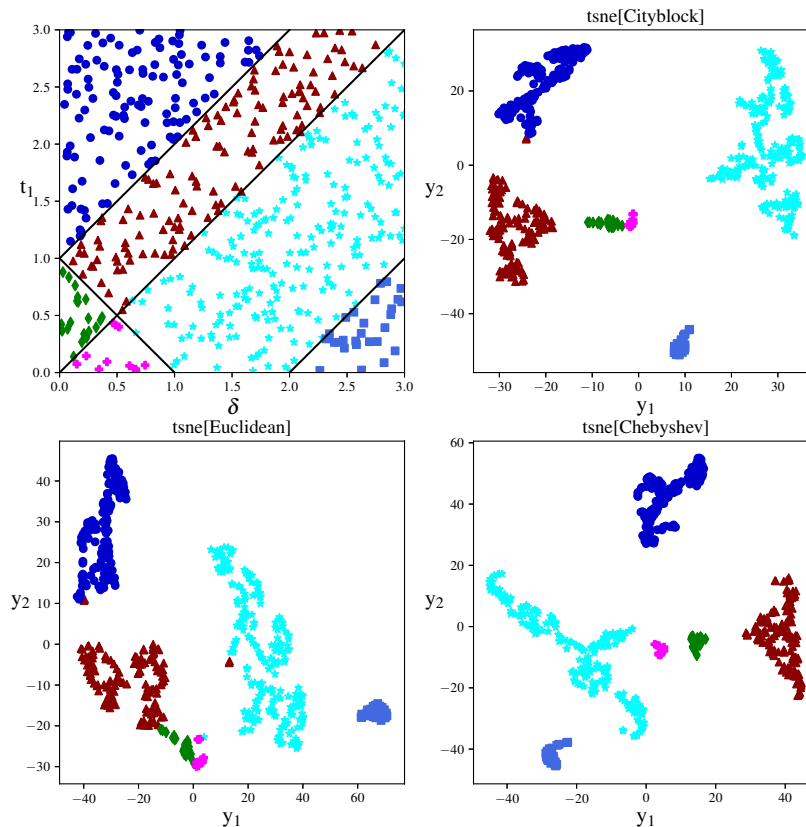


Figure 6. tSNE mapping of the non-Hermitian extended SSH model using different distance functions. Top-left: Points in the $\delta - t_1$ parameter space with $t_2, t_3 = 1$ at which input Bloch vectors are calculated. The other panels show tSNE output using the distance function indicated in the panel title in Eq. 1.

The choice of distance function used in constructing the probability distribution Eq. 1 in the input space can affect the mapping in the reduced space. As an example the case of the non-Hermitian extended SSH model is presented here. Bloch vectors at 529 points selected in the range $0 \leq \delta, t_1 \leq 3$ with $t_2, t_3 = 1$ were used as input. These are plotted in the top-left panel of Fig. 6. The black lines show phase boundaries. The other panels show the tSNE mapping to two-dimensional space where the distance function used is indicated in the panel title. Cityblock is the scikit-learn name for the \mathbb{L}_1 norm. Only the Chebyshev distance leads to a usable clustering corresponding to the different regions of the phase diagram. Cityblock clusters the points correctly but does not provide any separation between points mapped from the two small regions indicated by diamonds and +’s. In this example the input data are labeled to illustrate the effect of different distance functions. In an analysis where the input is not labeled separation of clusters from different regions is critical in order to identify phases correctly.

Scikit-learn provides a variety of distance functions but sometimes a custom distance function may have to be crafted in order to get good results. Fig. 7 shows the tSNE mapping of the SSH model for wavefunction input using different distance functions as indicated in the panel titles. This model has two phases so in the reduced space one would expect to see two clusters of points if tSNE is identifying the phases correctly. This is not the case using the

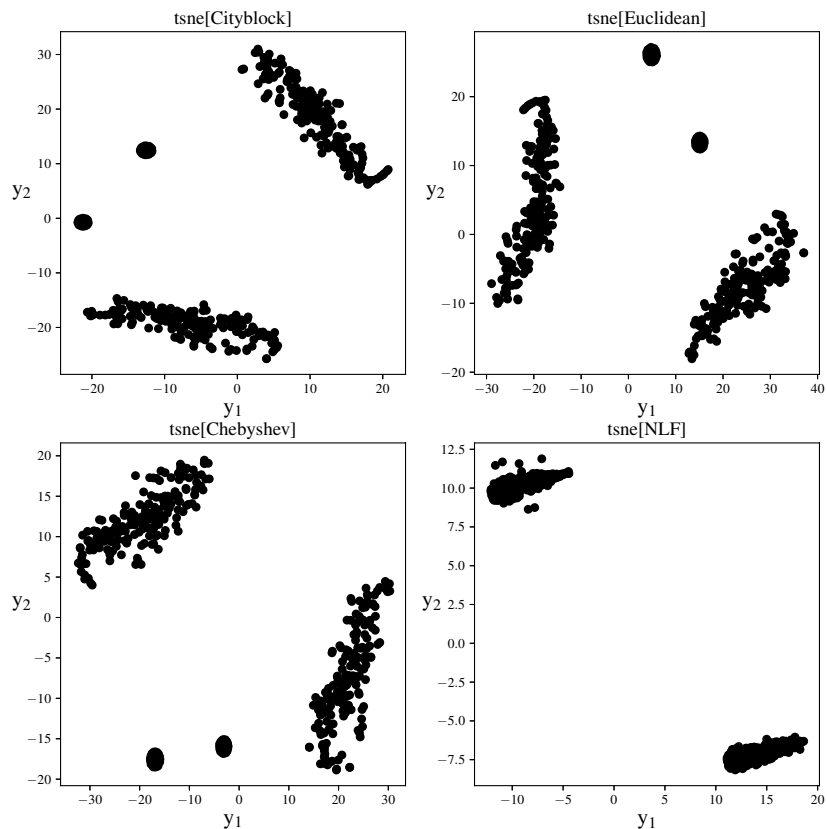


Figure 7. tSNE mapping of the SSH model with wavefunction input using the distance function indicated in the panel title in Eq. 1.

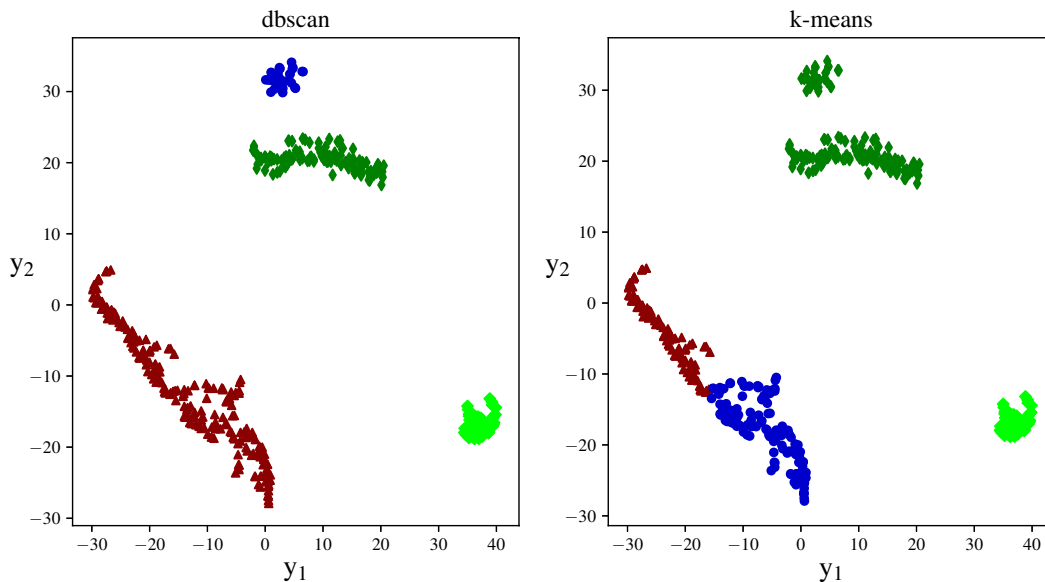


Figure 8. Comparison of dbSCAN and k-means clustering of tSNE output for the extended SSH model shown in the top-right panel of Fig. 2.

Cityblock, Euclidean and Chebyshev distances. A binary classification of the points is problematic. However, using the custom distance function, negative logarithmic fidelity [23], Eq. 14, gives two reasonably compact well-separated clusters.

Appendix B: k-means versus dbscan

After mapping of the input data to a reduced space one would like to identify clusters of points sharing some common features. This could be done by inspection but better would be to have an algorithmic procedure which more objective. However, this can lead to a problem if the choice of clustering algorithmic is not appropriate. An example is shown in Fig. 8.

The two panels show the clusters, indicated by different symbols and colors, returned by the dbscan and k-means clustering algorithms [41] for the tSNE output of the extended SSH model (top-right panel of Fig. 2). The tSNE output has well separated clusters but they are not particularly compact. The k-means clustering algorithm, which calculates distances from a set of centroids, fails in this case where there is a cluster that is quite extended. On the other hand, dbscan, which analyzes the data by dividing it into subgroups based on the density of points, gives the correct identification of clusters associated with different regions of the phase diagram as shown in Fig. 2.

-
- [1] P. Mehta *et al.*, *Physics Reports* **810**, 1 (2019).
 - [2] G. Carleo *et al.*, *Reviews of Modern Physics* **91**, 045002 (2019).
 - [3] P. T. Komiske, E. M. Metodiev and M. D. Schwartz, *Journal of High Energy Physics* **2017**, 110 (2017).
 - [4] E. M. Metodiev, B. Nachman and J. Thaler, *Journal of High Energy Physics* **2017**, 174 (2017).
 - [5] A. Butter, G. Kasieczka, T. Plehn and M. Russell, *SciPost Physics* **5**, 028 (2018).
 - [6] M. Farina, Y. Nakai and D. Shih, *Physical Review D* **101**, 075021 (2020).
 - [7] J. Hajer, Y.-Y. Li, T. Liu and H. Wang, *Physical Review D* **101**, 076015 (2020).
 - [8] C. J. Fluke and C. Jacobs, *WIREs Data Mining and Knowledge Discovery* **10**, e1349 (2019).
 - [9] S. J. Wetzel, *Physical Review E* **96**, 022140 (2017).
 - [10] J. Carrasquilla and R. G. Melko, *Nature Physics* **13**, 431 (2017).
 - [11] E. P. L. van Nieuwenburg, Y.-H. Liu and S. D. Huber, *Nature Physics* **13**, 435 (2017).
 - [12] M. S. Scheurer and R.-J. Slager, *Physical Review Letters* **124**, 226401 (2020).
 - [13] S. J. Wetzel and M. Scherzer, *Physical Review B* **96**, 184410 (2017).
 - [14] P. Suchsland and S. Wessel, *Physical Review B* **97**, 174435 (2018).
 - [15] P. Huembeli, A. Dauphin and P. Wittek, *Physical Review B* **97**, 134109 (2018).
 - [16] N. Yoshioka, Y. Akagi and H. Katsura, *Physical Review B* **97**, 205110 (2018).
 - [17] L. Wang, *Phys. Rev. B* **94**, 195105 (2016).
 - [18] W. Hu, R. R. P. Singh and R. T. Scalettar, *Physical Review E* **95**, 062122 (2017).
 - [19] P. Ponte and R. G. Melko, *Physical Review B* **96**, 205146 (2017).
 - [20] J. F. Rodriguez-Nieva and M. S. Scheurer, *Nature Physics* **15**, 790 (2019).
 - [21] J. Wang, W. Zhang, T. Hua and T.-C. Wei, *Unsupervised learning of topological phase transitions using calinski-harabaz index*, 2020, [arXiv:2010.06136].
 - [22] Y. Long, J. Ren and H. Chen, *Physical Review Letters* **124**, 185501 (2020).
 - [23] Y. Yang, Z.-Z. Sun, S.-J. Ran and G. Su, *Visualizing quantum phases and identifying quantum phase transitions by nonlinear dimensionality reduction*, 2020, [arXiv:2006.08461].
 - [24] C.-K. Chiu, J. C. Y. Teo, A. P. Schnyder and S. Ryu, *Rev. Mod. Phys.* **88**, 035005 (2016).
 - [25] Y. Che, C. Gneiting, T. Liu and F. Nori, *Physical Review B* **102**, 134213 (2020).
 - [26] L.-F. Zhang *et al.*, *Machine learning topological invariants of non-hermitian systems*, 2020, [arXiv:2009.04058].
 - [27] B. Narayan and A. Narayan, *Machine learning non-hermitian topological phases*, 2020, [arXiv:2009.06476].
 - [28] A. Kerr, G. Jose, C. Riggert and K. Mullen, *Automatic learning of topological phase boundaries*, 2020, [arXiv:2010.13236].
 - [29] L.-W. Yu and D.-L. Deng, *Unsupervised learning of non-hermitian topological phases*, 2020, [arXiv:2010.14516].
 - [30] N. Käming *et al.*, *Unsupervised machine learning of topological phase transitions from experimental data*, 2021, [arXiv:2101.05712].
 - [31] W. P. Su, J. R. Schrieffer and A. J. Heeger, *Phys. Rev. Lett.* **42**, 1698 (1979).
 - [32] W. P. Su, J. R. Schrieffer and A. J. Heeger, *Phys. Rev. B* **22**, 2099 (1980).
 - [33] J. K. Asbóth, L. Oroszlány and A. Pályi, *Lecture Notes in Physics* (2016).
 - [34] N. Batra and G. Sheet, *Resonance* **25**, 765 (2020).
 - [35] H.-C. Hsu and T.-W. Chen, *Physical Review B* **102**, 205425 (2020).
 - [36] L. Li, Z. Xu and S. Chen, *Physical Review B* **89**, 085111 (2014).
 - [37] C. Yin, H. Jiang, L. Li, R. Lü and S. Chen, *Physical Review A* **97**, 052115 (2018).
 - [38] L. van der Maaten and G. Hinton, *Journal of Machine Learning Research* **9**, 2579 (2008).

- [39] F. Pedregosa *et al.*, Journal of Machine Learning Research **12**, 2825 (2011).
- [40] <https://scikit-learn.org/stable/modules/manifold.html>.
- [41] <https://scikit-learn.org/stable/modules/clustering.html>.
- [42] E. Schubert, J. Sander, Martin, H.-P. Kriegel and X. Xu, ACM Transactions on Database Systems **42**, 19 (2017).